LONG-TERM TIMING OF PULSARS IN NGC 6440: AN UPDATED MASS LIMIT OF MILLISECOND PULSAR J1748-2021B

Author:
Nick Clifford

Advisor: Dr. Scott M. Ransom
National Radio Astronomy Observatory

This thesis is submitted in partial completion of the requirements of the BS Astronomy-Physics Major.

University of Virginia
Department of Astronomy
10 May 2019

Draft version May 13, 2019
Typeset using LaTeX **twocolumn** style in AASTeX62

LONG-TERM TIMING OF PULSARS IN NGC 6440: AN UPDATED MASS LIMIT OF MILLISECOND PULSAR J1748-2021B

Nicholas Clifford[1] and Scott M. Ransom[2,1]

[1] *University of Virginia, Department of Astronomy, P.O. Box 400325, Charlottesville, VA 22904, USA*
[2] *National Radio Astronomy Observatory, 520 Edgemont Rd., Charlottesville, VA 22903, USA*

ABSTRACT

After 11 years of continued observations with the Green Bank Telescope (GBT), we present updated timing solutions of 6 previously published pulsars in NGC 6440. We obtain improvements in timing parameters that allow us to better describe the dynamics of the cluster, such as measure the proper motion of the pulsars and and estimate the cluster's motion ($\mu_\alpha = -1.04(20)\,\mathrm{mas\ yr^{-1}}$, $\mu_\delta = -3.0(2.5)\,\mathrm{mas\ yr^{-1}}$). Using additional observing bandwidth, we measure the flux densities and spectral indices of each pulsar and investigate the effects of refractive scintillation on the variance of each pulsar's flux density as a function of observing frequency. For the eccentric binary millisecond pulsar (MSP) NGC 6440B, we report on a much more precise rate of periastron advance, $\dot{\omega} = 0.003684(21)^\circ\,\mathrm{yr^{-1}}$, which if purely relativistic, would indicate a total system mass of 2.675 ± 0.022 and a median pulsar mass of $2.548^{+0.047}_{-0.078}\,M_\odot$ assuming random inclinations. We also measure the rate of periastron advance for NGC 6440F ($\dot{\omega} = 0.0673(28)^\circ\,\mathrm{yr^{-1}}$) despite its incredibly low flux density ($S_{1.5} = 0.019\,\mathrm{mJy}$).

Keywords: binaries: general – equation of state – globular clusters: individual (NGC 6440) – pulsars: general – stars: neutron

1. INTRODUCTION

Millisecond pulsars (MSPs) make up an extraordinary subset of radio pulsars that have much shorter spin periods than a 'normal' pulsar. These MSPs have much lower spin-down rates, implying that they have weaker magnetic fields and larger characteristic ages. This makes them robust probes of astrophysical phenomena that require long-term timing

MSPs are also known as 'recycled' pulsars since they result from the interaction between a neutron star (NS) and another low mass star in a close binary. When close enough, the star will accrete mass onto the pulsar in a low-mass x-ray binary (LMXB), causing the pulsar to spin up to frequencies of hundreds of Hz. Thus, globular clusters' (GCs) high stellar density make them perfect factories of MSPs since they allow for greater stellar interactions that can produce compact binaries with other main sequence stars. Additionally, GCs host a higher fraction of MSPs since they are old stellar systems where any regular pulsars would most likely have already become inactive NSs (Prager et al. 2017).

The motivation to search NGC 6440 for pulsars by Freire et al. (2008) was due to the large Γ_C, which represents the correlation between x-ray point sources and the rate of stellar encounters within the GC core (Pooley et al. 2003). NGC 6440 was found to be one of six GCs with the largest Γ_C values, which would indicate a high rate of LMXB formation and a subsequent high rate of MSP formation. One pulsar had been known to be likely within the cluster: PSR B1745-20A (NGC 6440A; Lyne et al. (1996)). At the time, technological improvements in instrumentation, specifically the Green Bank Telescope's (GBT) S-Band receiver with the Pulsar Spigot, allowed for better detection of MSPs, which resulted in the discovery of 5 additional MSPs.

Since the Freire et al. (2008) study, more than a decade's worth of observations have been carried out as part of a series of long-term timing observations for pulsars in bulge globular clusters (Prager et al. 2017; Bilous et al. 2018; DeCesar et al. 2015). In this paper we present all of the pulsars' original timing solutions as well as improvements to the binary parameters for the three binary pulsars in the cluster.

ncc3ee@virginia.edu

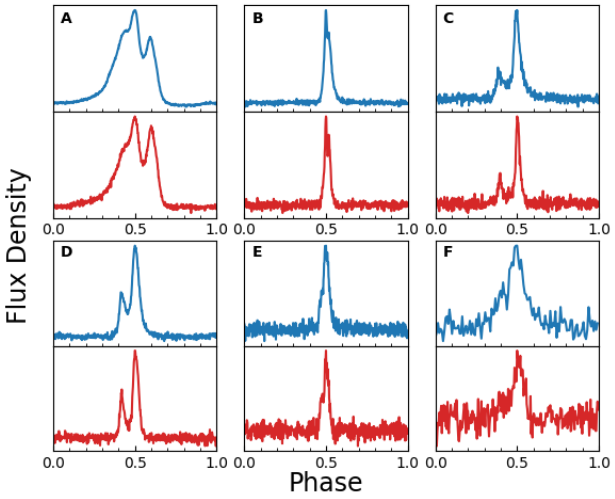

Figure 1. The averaged summed profiles of each pulsar over one full rotation. They are obtained by summing together each pulsar's GUPPI observations at 1.5 GHz (blue) and 2 GHz (red).

1.1. *Observations*

Before 2009, the GBT's Pulsar Spigot Spectrometer (Kaplan et al. 2005) and S-band receiver (with usable bandwidth between ∼1650−2250 MHz) were used for timing observations to record data every 81.92 μs with 1024 frequency channels over a total of 800 MHz of bandwidth (768 channels over the usable band). On two occasions, observations were made at 820 MHz with a bandwidth of 50 MHz to more accurately determine dispersion measures (DM) and search for additional steep-spectrum pulsars. See Freire et al. (2008) for more details about these early observations.

Since late 2009, we have observed the cluster with The Green Bank Ultimate Pulsar Processing Instrument (GUPPI; DuPlain et al. (2008)) using coherent dedispersion within each of 512 frequency channels at a DM of 223 pc cm^{-3}, which is the approximate average DM of the cluster pulsars. Spectra with full polarization information were dumped every 10.24 μs. Before each cluster observation, standard polarization calibration scans were made with a pulsed noise diode while pointing towards the cluster. Several flux calibration observations of quasars were also made, or used from other projects (see §2). The observations have used both the L-band (i.e. 1.1-1.9 GHz) and S-band (i.e. 1.6-2.4 GHz, with approximately the top ∼0.7 GHz usable) receivers in order to improve measurements of the DMs of the pulsars.

2. TIMING ANALYSIS

Individual timing scans and TOAs were processed using `PSRCHIVE` (Hotan et al. 2004; van Straten et al. 2012) in two iterations. The raw GUPPI observation data were calibrated using the `pac` command. Each file was examined using `psrzap` to remove RFI and averaged to a single frequency channel and 2 or more sub-integrations using `pam`. The first iteration of TOAs were fitted to an artificial profile, obtained by fitting a set of Gaussian distributions to the original Spigot summed profiles provided by Freire et al. (2008), using `pat`. In order to determine orbital phase information for binary pulsars NGC 6440B and NGC 6440D, we generated TOAs every 600 seconds of observing time. As for the fainter pulsar binary system (NGC 6440F) and the isolated pulsars, only 2 TOAs per observation were generated. These TOAs were fitted to the original ephemeris determined by Freire et al. (2008) and updated to include fits for proper motion and higher order frequency derivative parameters.

For the second iteration, each GUPPI observation was re-aligned with the updated timing model using `pam` and the process was repeated. We used `rmfit` to determine the rotation measure (RM) from each observation of the pulsars with the highest flux density (NGC 6440A & NGC 6440B) and found an average RM value of -8.7 rad m^{-2}. We assume this value to be an RM estimate GC, which is used to correct RFI removed observation files with `pam`. Two new standard profiles were generated for each pulsar by summing together L-band and S-band RM corrected observations separately with `psradd` and `ppalign` (Figure 1). Templates were made by smoothing these profiles using the adaptive wavelet-based smoothing process offered by `psrsmooth`. Both Spigot and GUPPI TOAs were regenerated using their corresponding frequency dependent templates and were fitted to a final pulsar model after removing outliers. As the absolute timing offsets between the Spigot and GUPPI are known to be $\lesssim$1 μs, which is much smaller than the timing precision for any of these pulsars, no timing JUMPs were fit between the old and new data.

The parameters obtained from the timing fits are included in Tables 1 and 2. To account for the motion of the telescope relative to the solar system barycenter, we used the DE436 solar system ephemeris. The time system used is Barycentric Dynamical Time (TDB). Parameter uncertainties quoted in Tables 1 and 2 are 1-σ uncertainties estimates on measured `TEMPO` parameters, however global error factors (EFAC) were applied to TOAs so that the reduced χ^2 value is approximately 1 after fitting. Due to the higher dynamic range of GUPPI and its factor of 8 improvement in time resolution compared to the Spigot, the computed EFACs for the Spigot data were much larger than those for GUPPI. Figure 2 shows the improvement in precision between the older and newer TOAs (separated by the vertical dashed line).

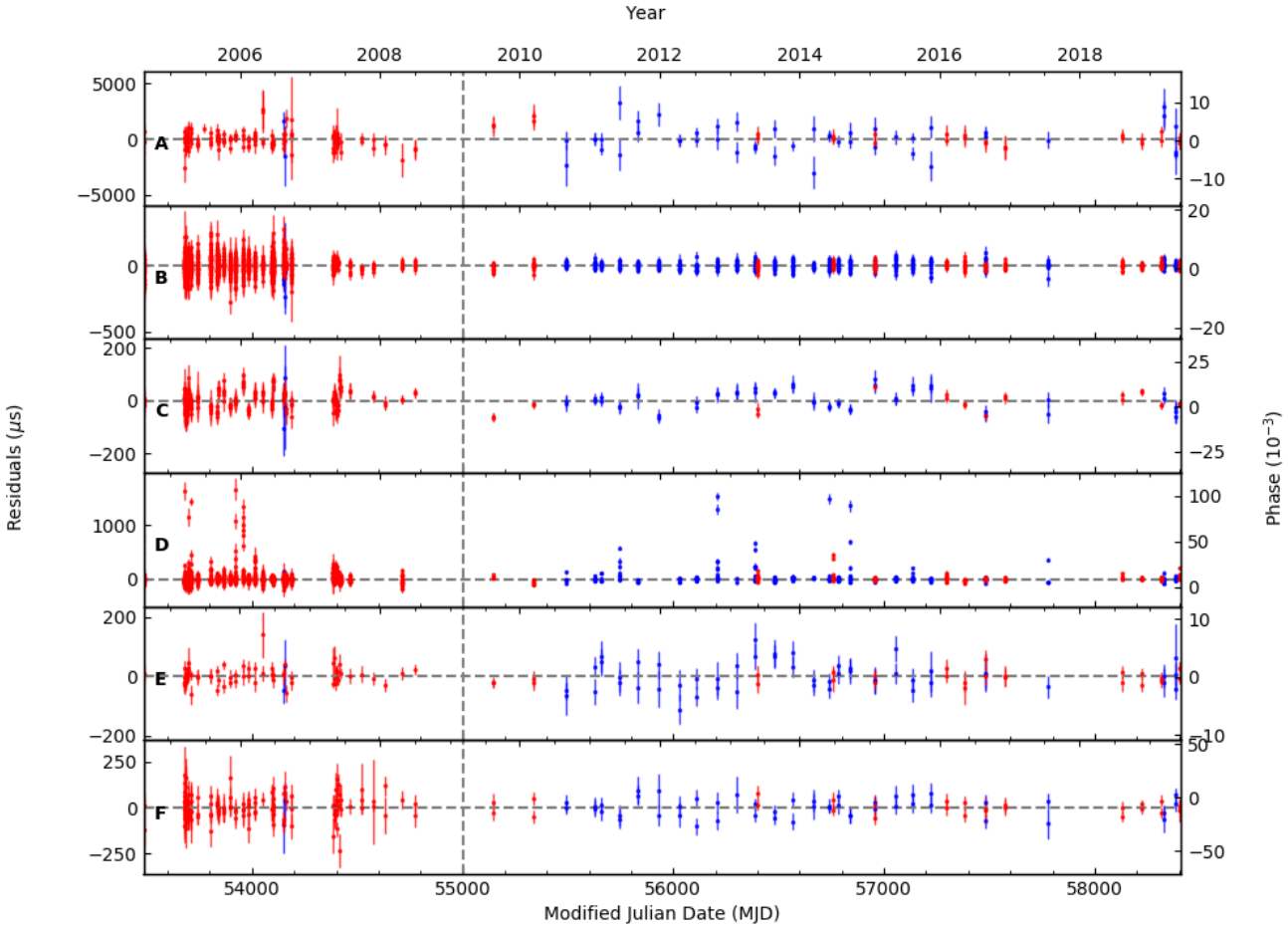

Figure 2. The TOA residuals as a function of time for each pulsar. The blue and red points indicate times of arrival at 1.5 GHz and 2 GHz respectively, while the vertical dashed line indicates the switch from Spigot to GUPPI backends.

2.1. *Notes on Individual Pulsars*

Previously discovered by Lyne et al. (1996), NGC 6440A was the only known pulsar in the GC before the searches described by Freire et al. (2008). It is an isolated pulsar with a period of 288.6 ms, considerably longer than the rest of the pulsars in question. When folding the observations, RFI is averaged throughout the pulse phase. With this much slower pulsar, there is less averaging, and its pulse profiles are much more contaminated with RFI compared to the other pulsars.

As described by Freire et al. (2008), NGC 6440C contains notably larger EFACs compared to rest of the pulsars indicating the presence of an unmodeled effect within our timing solution. With the addition of the GUPPI data, an obvious systematic effect can be observed within the residual plot (Figure 2). The possible causes of this effect will be discussed in a later section.

NGC 6440D is an eclipsing binary system with a orbital period of about 6.9 hours. Plotting its TOA residuals as a function of orbital phase, we can observe the affected TOAs during its eclipse, which lasts for about 10% of its orbit. During eclipse, TOAs are delayed by approximately ~ 1 ms. Figure 3 shows the level to which our observations have covered the pulsar's orbit. Using the `TEMPO` BTX model, the pulsar's orbital motion is expressed in frequency derivatives as a Taylor Expansion around its epoch of periastron passage in Table 2.

3. DISCUSSION

3.1. *Spectral Index*

Due to the increase in band coverage since the Freire et al. (2008) study, we have measured each pulsar's flux density in both bands and compare them to previous results. As part of the process, we also estimate the

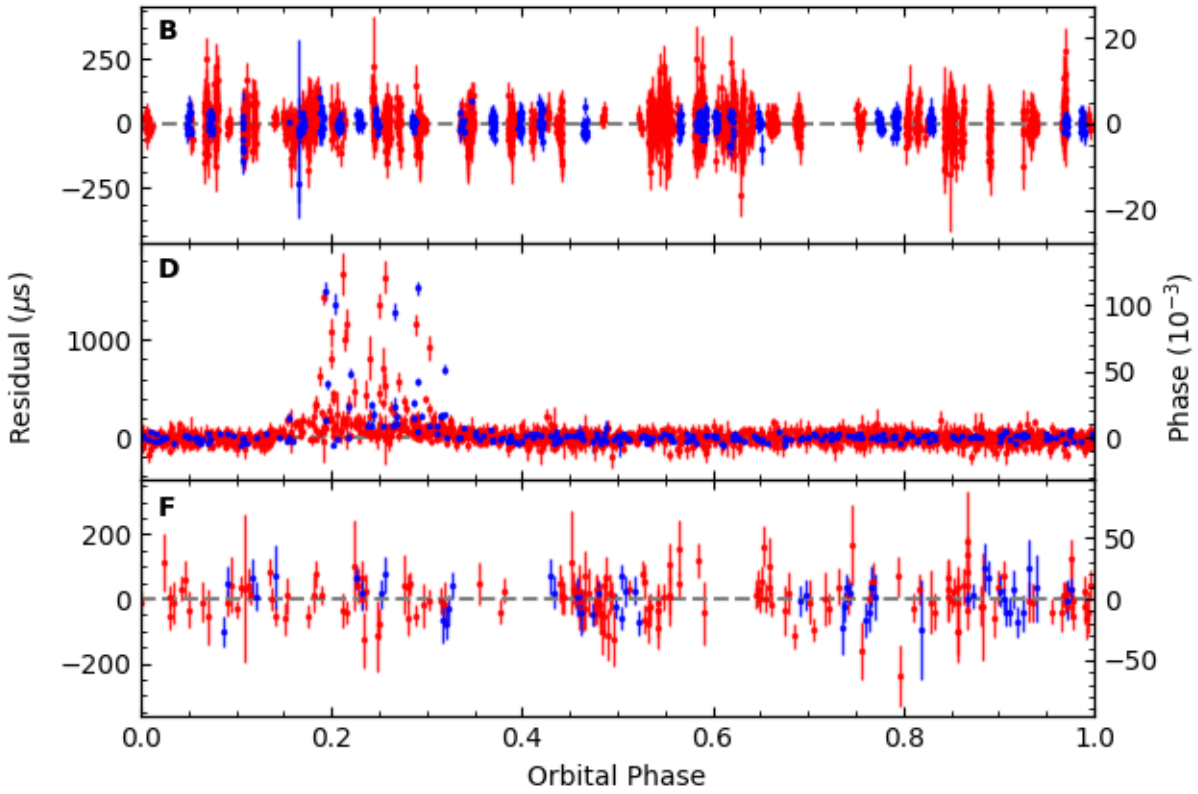

Figure 3. The TOA residuals as a function of orbital phase for each binary pulsar.

spectral index of each pulsar, and investigate the effects of refractive scintillation on our measurements.

Since the observations were designed having a portion of both bands overlapping with one another, we are able to account for any offset inconsistencies in the flux density measurements that arise from differences in each band's calibration (Wang et al. 2018). First, we divided each of the GUPPI coherently dedispersed data into 8 subbands so that 2 pairs of L & S-subbands overlap; we neglect the lowest S-subband as there is hardly any signal for each available observation, due to filters in the system. As the pulse profiles vary with flux density, as seen in Figure 1, the flux density measurements for each observation's subbands are calculated using the template matching algorithm provided by `psrflux`. We then compute an average flux density and standard deviation over all observations at that frequency to determine the best fit power-law spectra for each pulsar.

To correct for the band offset, we select a global scaling factor that when applied to either band's set of flux density values will result in the lowest squared residuals of our spectral fit. We found that reducing L-band and increasing S-band values by 20% resulted in the best fit. Given the offset uncertainties between bands and the stability of the system, we trust these average flux measurements to about 20%. Additionally, the internal data taking software of the GUPPI coherently dedispersed data changes the scaling data by a factor of 20. Therefore, we correct for this by also multiplying all flux density measurements by 20.

Once we applied the necessary scaling adjustments for either band and fit for spectral index, we found only 2 pulsars had $\alpha < -1$ (NGC 6440A & B) and one to have $\alpha > 0$ (NGC 6440C). These results support the claim made by (Bates et al. 2013) that the observing bandwidth of pulsar search surveys is a preferential selector of a pulsar's spectral index and any other properties correlated with it (characteristic age, magnetic field). In our case, we expect to see more pulsars with shallower spectral indices because these pulsars were discovered at higher radio frequencies (2 GHz). Additionally, we measured NGC 6440A index to be the steepest of all the pulsars: $\alpha \sim -1.7$. As mentioned in §2.1, the only pulsar not part of the Freire et al. (2008) survey was

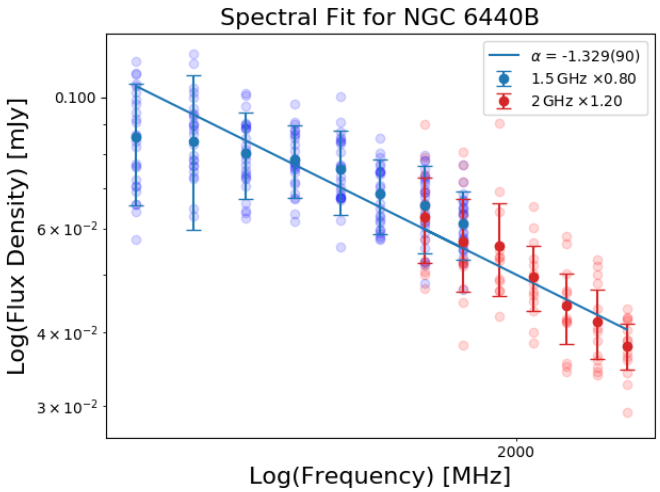

Figure 4. Spectral fit for NGC 6440B after applying the necessary scaling adjustments for either band. Includes the individual measurements for each observation as well as the average at each subband

NGC 6440A, which discovered by Lyne et al. (1996) in a survey of globular clusters at a lower frequency of 650 MHz.

The flux densities at 1.5 and 2 GHz ($S_{1.5}$, S_2) are listed in Tables 1 and 2, which were found by finding the average flux density of the subbands adjacent to the bands center frequency. We note that for each pulsar, we measure a flux density at 2 GHz that is 10-50% larger than those predicted by Freire et al. (2008) from the radiometer equation and their total observing time. We believe to expect such results as we may be biased in having twice as many L-band GUPPI observations compared to S-band and are dominated by systematic errors in the bands' offset.

3.2. *Proper Motion*

As a result of the extended timing observations over the past 14 years, we have constructed updated timing models for each of the pulsars in the cluster. We found that proper motion was significant for the pulsars, and have included proper motion terms in the timing fits for each pulsar. However, we note that our observations of each pulsar's proper motion in declination is consistently less significant than the right ascension term due to the fact that the cluster is only $\sim 3^{\circ}$ from the Ecliptic plane.

Despite this, we test the process put forth by Freire et al. (2017) to use pulsar timing to determine the kinematics of the NGC 6440 cluster as a whole. Using a weighted average of each set of proper motion terms, we estimate the cluster's proper motion in right ascension (RA) and declination (DEC) to be: $-1.04(20)$ mas yr^{-1} & $-3.0(2.5)$ mas yr^{-1} respectively. Compared to more accurate globular cluster proper motion results obtained from the recent *Gaia* DR2 Gaia Collaboration et al. (2018), we find our proper motion estimates to agree with their kinematic measurements of NGC 6440: $\mu_\alpha = -1.21(11)$ mas yr^{-1} & $\mu_\delta = -3.88(10)$ mas yr^{-1}

3.3. *NGC 6440F*

NGC 6440F's system is a relatively normal MSP-white dwarf binary, however, our ability to model both its keplerian orbital and spin parameters is a feat to be highlighted. From Table 2, our flux density measurements of NGC 6440F are the lowest out of all the other pulsars in the cluster; the signal-to-noise in each of the GUPPI observations ranges only from a few to ~ 10.

Even so, we are able measure its spin rate, the fastest of all the pulsars, and its spin down rate, subsequently the lowest of the pulsars. Finally, from the combined data from the past decade, we observe the rate of advance of periastron to significant accuracy: $\dot{\omega} = 0.0067(3)^{\circ}\,\mathrm{yr}^{-1}$. This implies a minimum companion mass of $0.3\,M_{\odot}$. If due entirely to general relativity, which is likely for a white dwarf companion, we could estimate the median possible pulsar mass to about $\sim 1.47\,M_{\odot}$. However, our ability to detect a relativistic orbital parameter of this pulsar given its short spin period, highly dispersed radio signal, and very low flux density is an account to the efficacy of long-term pulsar timing.

3.4. *NGC 6440D*

Given NGC 6440D's eclipsing nature, small orbital period of ~ 6.9 hours, and minimum companion mass $\sim 0.12\,M_{\odot}$, we classify it as a eclipsing 'redback' (Roberts 2013). Mentioned in §2.1, it has a highly variable orbit that must be expressed as orbital frequency polynomials within our timing model. Therefore, we are unable to derive the eccentricity simply from timing. However, it is fortunate that after 14 years worth of observations, we are still capable of constructing a fully phase connected timing solution for this pulsar. Figure 3 shows how this is capable, as our orbital timing coverage indicates that we still detect TOAs during the eclipse.

We use the first order orbital frequency derivative as our observed $\dot{P}_b$. Then, we investigate as to whether the pulsar's acceleration due to the cluster is significantly larger than all line of sight accelerations, overwhelming our detection of the intrinsic $\dot{P}$ and $\dot{P}_b$. We list the acceleration terms contributing to our observed spin period change of $\dot{P}/P_{\rm obs}$ (Phinney 1993).

$$\left(\frac{\dot{P}}{P}\right)_{\rm obs} = \left(\frac{\dot{P}}{P}\right)_{\rm int} + \frac{a_c}{c} + \frac{a_g}{c} + \frac{a_s}{c} \qquad (1)$$

Here, $\dot{P}/P_{\rm int}$ is the pulsar's intrinsic spin period change associated with intrinsic spin down rate, a_c is the line of sight acceleration due to the cluster, a_g is the acceleration due to the galactic potential, and a_s is the centrifugal acceleration due to the proper motion and distance of the cluster ($\mu^2 D$) (Shklovskiĭ 1970). In order to circumvent the need to measure $\dot{P}/P_{\rm int}$, we follow the process of Prager et al. (2017) to predict the intrinsic spin period change using our measured P and an assumed magnetic surface field strength B. The typical $\dot{P}$ for an MSP is given as:

$$c\left(\frac{\dot{P}}{P}\right)_{\rm int} = 7.96\times10^{-10}\left(\frac{B}{2\times10^8\,{\rm G}}\right)\left(\frac{2\,{\rm ms}}{P}\right)^2 {\rm m\,s^{-2}} \quad (2)$$

Here, we assume a magnetic field strength of MSPs similar to NGC 6440D from the ATNF catalogue[1] (Manchester et al. 2016). Given spin rate of ~ 13 ms and its redback nature, we assume B to be 2×10^9 G and measure the predicted spin period change as $\sim 10^{-17}\,s^{-1}$. Using (1), we find the acceleration contribution from the cluster to be of the same magnitude, suggesting that the system is not solely dominated by the cluster. Next, we express the orbital period derivative in a similar form as Eqn. (1). This result is validated by the nature of redbacks and the pulsar's tight, wandering orbit.

3.5. *NGC 6440B*

Mentioned previously in Freire et al. (2008), NGC 6440B is a very interesting binary MSPs, having an high orbital eccentricity (∼0.6) and a well behaved timing solution. This orbital nature us to measure its rate of advance of periastron to significant accuracy. We report this new value of $\dot{\omega} = 0.003684(21)^\circ\,{\rm yr}^{-1}$; a factor of 6 improvement in uncertainty since its previous publication. This value implies a new total system mass of $2.690 \pm 0.071\,M_\odot$. Assuming that the probability distribution of $\dot{\omega}$ is normal and that random inclination angles i are expressed by a uniform probability distribution for $\cos i$ ($0^\circ < i < 90^\circ$), we derive a median mass and 1σ mass limit of $2.548^{+0.047}_{-0.078}\,M_\odot$ and a minimum companion mass of $0.079\,M_\odot$.

Figure 5 shows the difference in NGC 6440B's mass distributions and the constraint improvements since its previous publication. Its new total system mass, lower than previously thought, still lies within the range of known double neutron star systems (DNS) (Faulkner et al. 2005; Weisberg & Taylor 2003). This could suggest that the end product of a DNS merger could be stable super-massive NS system. This would have created a substantial amount of heavier elements as research suggests DNS mergers are one of the most dominant r-process sites in the universe (Rosswog et al. 2018). If this correctly describes the origin of NGC 6440B, it may be possible to detect residual effects of the coalescence by observing the metalicities of stars in NGC 6440 in order to find pollution of r-process elements within their atmospheres.

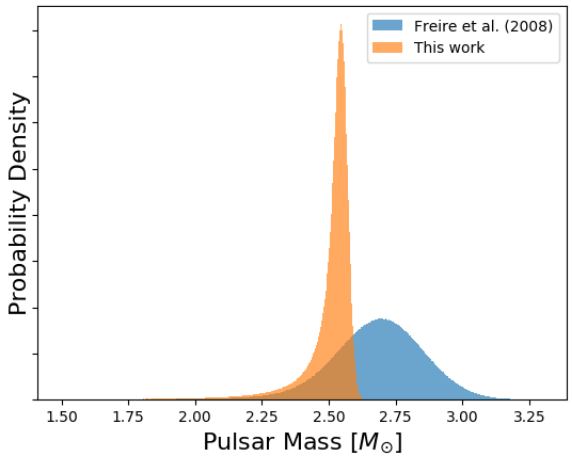

Figure 5. The mass distributions of NGC 6440B based on the previous timing model of Freire et al. (2008) and its updated counterpart assuming, assuming general relativity causes $\dot{\omega}$ and random inclinations of the orbit ($0^\circ < i < 90^\circ$).

This argument does assume, however, that the observed $\dot{\omega}$ is fully relativistic. Additionally, Figure 5 also features a new low mass tail that covers the same mass range of canonical pulsars $\sim$ 1.5-2 $M_\odot$. Previously there was a less than 1% chance that the mass of the pulsar was below 2 $M_\odot$, whereas that percentage has grown to With continued observations, we are still unable to successfully detect any evidence of Einstein delay γ, which would have allowed for improved mass estimates or constrained the level of possible contamination of $\dot{\omega}$ via classical effects.

4. CONCLUSION

We have been observing the 6 pulsars in NGC 6440 for the past 14 years and have constructed an up-to-date timing solution since Freire et al. (2008) for each pulsar. We have increased accuracy in all originally known parameters and are able to observe new parameters such as second spin frequency derivative ($\ddot{\nu}$) and proper motions in RA (μ_α); measurements of proper motion in DEC (μ_δ) are less significant. Even so, we are able to estimate the proper motion of the cluster as a whole using the proper motion terms from each pulsar

[1] http://www.atnf.csiro.au/research/pulsar/psrcat/

($\mu_\alpha = -1.04(20)\,\mathrm{mas\,yr^{-1}}$, $\mu_\delta = -3.0(2.5)\,\mathrm{mas\,yr^{-1}}$), which agrees with results from the recent Gaia Data Release (Gaia Collaboration et al. 2018). The third spin frequency derivative ($\ddot{\nu}$) is also detectable for half of the pulsars.

For the binary MSPs, improvements have been made towards measuring post-keplerian parameters for two of the pulsars. Despite its faint detection, we observe the rate of periastron advance ($\dot{\omega}$) of NGC 6440F to significant precision. NGC 6440B's updated mass limit of $2.532^{+0.057}_{-0.38}\,M_\odot$ still places it as potentially the most massive NS to date. Our inability to detect other relativistic effects such as Einstein delay (γ) or the rate of change of semi-major axis ($\dot{x}$) forces us to investigate other suggestions of its origin. Any ability to measure the relativistic effects of Shapiro delay would only be possible if the system's orbital inclination is edge on, which support the claim that the pulsar mass is much more massive than its companion. In addition, the new total mass of the system still makes it a reasonable product of DNS coalescence. Until its mass has been significantly constrained and agreed upon, future efforts to measure anomalous amounts of heavier elements within the cluster might serve as evidence of NGC 6440B's origin.

The National Radio Astronomy Observatory is a facility of the National Science Foundation operated under cooperative agreement by Associated Universities, Inc. The Green Bank Observatory is a facility of the National Science Foundation operated under cooperative agreement by Associated Universities, Inc.

Facility: GBT

Software: PSRCHIVE (Hotan et al. 2004; van Straten et al. 2012), Tempo (Nice et al. 2015)

REFERENCES

Bates, S. D., Lorimer, D. R., & Verbiest, J. P. W. 2013, MNRAS, 431, 1352

Bilous, A., Ransom, S., & Demorest, P. 2018, arXiv e-prints, arXiv:1811.05766

DeCesar, M. E., Ransom, S. M., Kaplan, D. L., Ray, P. S., & Geller, A. M. 2015, ApJ, 807, L23

DuPlain, R., Ransom, S., Demorest, P., et al. 2008, in Proc. SPIE, Vol. 7019, Advanced Software and Control for Astronomy II, 70191D

Faulkner, A. J., Kramer, M., Lyne, A. G., et al. 2005, ApJ, 618, L119

Freire, P. C. C., Ransom, S. M., Bégin, S., et al. 2008, ApJ, 675, 670

Freire, P. C. C., Ridolfi, A., Kramer, M., et al. 2017, MNRAS, 471, 857

Gaia Collaboration, Helmi, A., van Leeuwen, F., et al. 2018, A&A, 616, A12

Hotan, A. W., van Straten, W., & Manchester, R. N. 2004, PASA, 21, 302

Kaplan, D. L., Escoffier, R. P., Lacasse, R. J., et al. 2005, PASP, 117, 643

Lyne, A. G., Manchester, R. N., & D'Amico, N. 1996, ApJL, 460, L41

Manchester, R. N., Hobbs, G. B., Teoh, A., & Hobbs, M. 2016, VizieR Online Data Catalog, B/psr

Nice, D., Demorest, P., Stairs, I., et al. 2015, Tempo: Pulsar timing data analysis, Astrophysics Source Code Library, , , ascl:1509.002

Phinney, E. S. 1993, in Astronomical Society of the Pacific Conference Series, Vol. 50, Structure and Dynamics of Globular Clusters, ed. S. G. Djorgovski & G. Meylan, 141

Pooley, D., Lewin, W. H. G., Anderson, S. F., et al. 2003, ApJ, 591, L131

Prager, B. J., Ransom, S. M., Freire, P. C. C., et al. 2017, ApJ, 845, 148

Roberts, M. S. E. 2013, in IAU Symposium, Vol. 291, Neutron Stars and Pulsars: Challenges and Opportunities after 80 years, ed. J. van Leeuwen, 127–132

Rosswog, S., Sollerman, J., Feindt, U., et al. 2018, A&A, 615, A132

Shklovskiĭ, I. S. 1970, Soviet Physics Uspekhi, 12, 808

van Straten, W., Demorest, P., & Oslowski, S. 2012, Astronomical Research and Technology, 9, 237

Wang, Y., Ransom, S. M., Hessels, J. W. T., Stairs, I., & Freire, P. 2018, in American Astronomical Society Meeting Abstracts, Vol. 231, American Astronomical Society Meeting Abstracts #231, 243.16

Weisberg, J. M., & Taylor, J. H. 2003, in Astronomical Society of the Pacific Conference Series, Vol. 302, Radio Pulsars, ed. M. Bailes, D. J. Nice, & S. E. Thorsett, 93

Table 1. Parameters for the Isolated Pulsars

Parameter	PSR B1748−2021A	PSR J1748−2021C	PSR J1748−2021E
Data Reduction			
S_2 (mJy)	0.56	0.048	0.032
$S_{1.5}$ (mJy)	0.84	0.069	0.031
Span of Timing Data (MJD)	53478−58402	53478−58402	53478−58402
Number of TOAs	204	268	148
RMS TOA Residual (μs)	563.1	33.4	25.6
Spigot EFAC	1.5	2.8	1.16
GUPPI EFAC	3.9	2.3	1.44
Reference Epoch (MJD)	56000	56000	56000
Timing Parameters			
Right Ascension (RA, J2000)	$17^{\rm h}\ 48^{\rm m}\ 52\overset{\rm s}{.}685(2)$	$17^{\rm h}\ 48^{\rm m}\ 51\overset{\rm s}{.}17294(7)$	$17^{\rm h}\ 48^{\rm m}\ 52\overset{\rm s}{.}8001(1)$
Declination (DEC, J2000)	$-20\ 21'\ 39\overset{''}{.}8(7)$	$-20\ 21'\ 53\overset{''}{.}88(2)$	$-20\ 21'\ 29\overset{''}{.}36(3)$
Proper Motion in RA (mas yr^{-1})	-5(7)	-0.4(2)	-1.0(3)
Proper Motion in DEC (mas yr^{-1})	$0(1)\times10^{2}$	-13(4)	0(6)
Pulsar Period (ms)	288.6028606969(4)	6.2269327100863(2)	16.2640034650597(9)
Pulsar Frequency (Hz)	3.464969119105(5)	160.592710176587(6)	61.485476324960(3)
Frequency Derivative (Hz s^{-1})	$-4.7897(1)\times10^{-15}$	$1.5511(2)\times10^{-15}$	$-1.17922(2)\times10^{-15}$
Frequency 2nd Deriv. (Hz s^{-2})	$2.63(8)\times10^{-26}$	$8(1)\times10^{-27}$	$1.02(6)\times10^{-26}$
Frequency 3rd Deriv. (Hz s^{-3})	...	$2.0(4)\times10^{-34}$	...
Dispersion Measure (pc cm^{-3})	220.4(2)	226.943(7)	224.18(1)

Table 2. Parameters for the Binary Pulsars

Parameter	PSR J1748−2021B	PSR J1748−2021D	PSR J1748−2021F
Data Reduction			
S_2 (mJy)	0.053	0.085	0.019
$S_{1.5}$ (mJy)	0.077	0.121	0.026
Span of Timing Data (MJD)	53478−58402	53478−58402	53478−58402
Number of TOAs	1616	1597	210
RMS TOA Residual (μs)	34.4	37.4	47.8
Spigot EFAC	1.67	1.7	1.44
GUPPI EFAC	1.026	0.8	1
Reference Epoch (MJD)	56000	56000	56000
Timing Parameters			
Right Ascension (RA, J2000)	$17^{\rm h}\ 48^{\rm m}\ 52\overset{\rm s}{.}95219(4)$	$17^{\rm h}\ 48^{\rm m}\ 51\overset{\rm s}{.}64601(4)$	$17^{\rm h}\ 48^{\rm m}\ 52\overset{\rm s}{.}3337(2)$
Declination (DEC, J2000)	$-20\ 21'\ 38\overset{''}{.}90(1)$	$-20\ 21'\ 7\overset{''}{.}43(1)$	$-20\ 21'\ 39\overset{''}{.}50(5)$
Proper Motion in RA (mas yr^{-1})	-1.5(1)	-0.9(1)	-1.0(5)
Proper Motion in DEC (mas yr^{-1})	-4(2)	2(3)	-14(9)
Pulsar Period (ms)	16.7601271627532(6)	13.4958205052680(3)	3.7936291130402(5)
Pulsar Frequency (Hz)	59.665418423695(2)	74.097013931806(2)	263.59983282567(3)
Frequency Derivative (Hz s^{-1})	$1.15839(4)\times10^{-15}$	$-3.22018(4)\times10^{-15}$	$7.621(2)\times10^{-16}$
Frequency 2nd Deriv. (Hz s^{-2})	$-6.37(2)\times10^{-26}$	$1.0(3)\times10^{-27}$	$4(4)\times10^{-27}$
Frequency 3rd Deriv. (Hz s^{-3})	$3.0(9)\times10^{-35}$	$-5(1)\times10^{-35}$	...
Dispersion Measure (pc cm^{-3})	220.927(3)	225.001(3)	220.40(1)
Binary Model	DD	BTX	DD
Orbital Period (days)	20.55000607(6)	0.2860686062(2)	9.8339747(2)
Orbital Period Deriv. (10^{-12})	$-7(3)\times10^{1}$	-83.0(8)	...
Projected Semi-Major Axis (lt-s)	4.473(7)	0.397204(1)	9.49(6)
Orbital Eccentricity	0.5701650(7)	$< 10^{-4}$ [a]	0.053108(1)
Longitude of Periastron (deg)	314.42(9)	...	191.51(7)
Epoch of Periastron (MJD)	56019.380892(4)	56000.2973882(3)	54005.80620(4)
Orbital Frequency (Hz)	...	$4.045908507(3)\times10^{-5}$	...
Orbital Frequency 1st Deriv. (Hz s^{-1})	...	$1.36(1)\times10^{-19}$	...
Orbital Frequency 2nd Deriv. (Hz s^{-2})	...	$-6.5(2)\times10^{-28}$	...
Orbital Frequency 3rd Deriv. (Hz s^{-3})	...	$-8.8(1)\times10^{-35}$	...
Orbital Frequency 4th Deriv. (Hz s^{-4})	...	$1.3(2)\times10^{-43}$	...
Orbital Frequency 5th Deriv. (Hz s^{-5})	...	$6.8(2)\times10^{-50}$	...
Orbital Frequency 6th Deriv. (Hz s^{-6})	...	$1(1)\times10^{-59}$	...
Orbital Frequency 7th Deriv. (Hz s^{-7})	...	$-3.3(1)\times10^{-65}$	...
Derived Parameters			
Mass Function ($M_\odot$)	0.000228(1)	0.000822201(9)	0.0095(2)
Total System Mass ($M_\odot$)	1.9(1)		
Min Companion Mass ($M_\odot$)	≥ 0.079	≥ 0.12	≥ 0.3
Characteristic Age (Gyr)	-0.82	0.36	-5.5
Spin-down Lumin, $\dot{E}$ (10^{34} ergs s^{-1})	-0.27	0.94	-0.79

NOTE—Numbers in parentheses represent 1-σ uncertainties in the last digit as determined by `TEMPO` using the DE436 Solar System Ephemeris for the timing parameters and 1-σ uncertainties for the other parameters. The time system used is Barycentric Dynamical Time (TDB). Minimum companion masses were calculated assuming a pulsar mass of $1.4\,M_\odot$. The total system mass and 68% centralconfidence ranges on the masses of the pulsar and its companion were determined assuming that $\dot{\omega}$ is due completely to general relativity, and a random orbital inclination (i.e. probability density is constant in $\cos i$).

[a] This is the 10-σ upper limit as determined by `TEMPO`after fitting for ω. All other timing parameters were determined with ω set to 0.